

A methodology for the computation of the macro-element stiffness matrix for the stress analysis of a lap joint with functionally graded adhesive properties

Benjamin Ordonneau, Eric Paroissien, Michel Salaün, Julien Malrieu, Alexandre Guigue, Sébastien Schwartz

▶ **To cite this version:**

Benjamin Ordonneau, Eric Paroissien, Michel Salaün, Julien Malrieu, Alexandre Guigue, et al.. A methodology for the computation of the macro-element stiffness matrix for the stress analysis of a lap joint with functionally graded adhesive properties. International Journal of Adhesion and Adhesives, 2020, 97, pp.0. 10.1016/j.ijadhadh.2019.102505 . hal-02539836

HAL Id: hal-02539836
https://hal.science/hal-02539836

Submitted on 10 Apr 2020

HAL is a multi-disciplinary open access archive for the deposit and dissemination of scientific research documents, whether they are published or not. The documents may come from teaching and research institutions in France or abroad, or from public or private research centers.

L'archive ouverte pluridisciplinaire **HAL**, est destinée au dépôt et à la diffusion de documents scientifiques de niveau recherche, publiés ou non, émanant des établissements d'enseignement et de recherche français ou étrangers, des laboratoires publics ou privés.



Open Archive Toulouse Archive Ouverte (OATAO)

OATAO is an open access repository that collects the work of some Toulouse researchers and makes it freely available over the web where possible.

This is an author's version published in: https://oatao.univ-toulouse.fr/25082

Official URL: https://doi.org/10.1016/j.ijadhadh.2019.102505

To cite this version :

Ordonneau, Benjamin and Paroissien, Eric and Salaün, Michel and Malrieu, Julien and Guigue, Alexandre and Schwartz, Sébastien A methodology for the computation of the macro-element stiffness matrix for the stress analysis of a lap joint with functionally graded adhesive properties. (In Press: 2019) International Journal of Adhesion and Adhesives. ISSN 0143-7496

Any correspondence concerning this service should be sent to the repository administrator: tech-oatao@listes-diff.inp-toulouse.fr

A methodology for the computation of the macro-element stiffness matrix for the stress analysis of a lap joint with functionally graded adhesive properties

Benjamin Ordonneau[1], Eric Paroissien[1,*], Michel Salaün[1,] Julien Malrieu[2], Alexandre Guigue[3], Sébastien Schwartz[1]

[1] *Institut Clément Ader (ICA), Université de Toulouse, ISAE-SUPAERO, INSA, IMT MINES ALBI, UTIII, CNRS, 3 Rue Caroline Aigle, 31400 Toulouse, France*

[2] *CETIM, 7 rue de la Presse, BP50802, 42952 Saint-Etienne Cedex 1, France*

[3] *DGA TA, 47 rue Saint-Jean, 31130 Balma, France*

*To whom correspondence should be addressed: Tel. +33561338438, E-mail: eric.paroissien@isae-supaero.fr

Abstract –The interest of functionally graded adhesives (FGA) is growing as it is a mean to increase a bonded joint strength without any modification of the initial design of the adherends. The behaviour of bonded joints with variable adhesive properties along the overlap can be predicted with a potentially time-costly Finite Element (FE) analysis. Dedicated numerical procedures and design tools for FGA bonded joints would increase. The objective of this paper is to offer a mesh-free method for the analysis of functionally graded joints. The technique is based on the macro-element (ME) method and Taylor expansion in power series (TEPS) are used to approach the shape functions of the ME. The method has been developed so far for 1D-bar and 1D-beam kinematics frameworks. This mesh-free_method and a Finite-Element analysis give similar results.

Keywords*: functionally graded adhesive; single-lap bonded joint, Taylor expansion in power series, variable modulus, stress distribution, joint design, finite element stress analysis*

NOMENCLATURE AND UNITS

A_j extensional stiffness (N) of adherend j

B_j extensional and bending coupling stiffness (N.mm) of adherend j

D_j bending stiffness (N.mm^2) of adherend j

D_T matrix of the recursive equation system with displacement boundary conditions

E_a adhesive peel modulus (MPa)

$E_{a,min}$ minimal adhesive shear modulus (MPa)

$E_{a,max}$ maximal adhesive shear modulus (MPa)

E_j adherend Young's modulus (MPa) of adherend j

F_e element nodal force vector

G_a adhesive shear modulus (MPa)

$G_{a,min}$ minimal adhesive shear modulus (MPa)

$G_{a,max}$ maximal adhesive shear modulus (MPa)

K stiffness matrix

K_{BBa} elementary stiffness matrix of a bonded-bars element

K_{BBe} elementary stiffness matrix of a bonded-beams element

L half-length (mm) of bonded overlap

L_T matrix with load boundary conditions

M_j bending moment (N.mm) in adherend j around the z-direction

N_j normal force (N) in adherend j in the x-direction

N_u number of terms in the series u after truncation

N_v number of terms in the series v after truncation

$Q_{i,j,k,l}$ nodal axial force of node i, j, k and l

$R_{i,j,k,l}$ nodal shear force of node i, j, k and l

$S_{i,j,k,l}$ nodal Moment force of node i, j, k and l

S adhesive peel stress (MPa)

T adhesive shear stress (MPa)

U_T vector of the unknown parameters of the displacements series

V_j shear force (N) in adherend j in the y-direction

b width (mm) of the adherends

e_a thickness (mm) of the adhesive layer

f magnitude of applied tensile force (N)

u_j displacement (mm) of adherend j in the x-direction

u_{j_n} n^{th} parameter of the axial displacement serie of the adherend j (mm^{-1})

$(u_j)_n$ dimensionless n^{th} parameter of the axial displacement serie of the adherend j

v_j displacement (mm) of adherend j in the y direction

v_{j_n} n^{th} parameter of the transverse displacement serie of the adherend j (mm^{-1})

$(v_j)_n$ dimensionless n^{th} parameter of the transverse displacement serie of the adherend j

θ_j bending angle (rad) of the adherend j around the z-direction

(x,y,z) global reference system of axes

BBa bonded-bars

BBe bonded-beams

FE Finite Element

FGA functionally graded adhesive

HA homogeneous adhesive

ME macro-element

ODE ordinary differential equation

TEPS Taylor expansion in power series

1. Introduction

The use of adhesively bonded joints increased over the last decade thanks to their high mechanical performances. They present a high strength-to-weight ratio, static and fatigue strength which makes them attractive for structural design **[1-3]**. Moreover, this technology allows dissimilar adherends assemblies. Contrary to mechanical fastening, the load transfer is spread along the bonded overlap instead of being localized at the position of the fasteners. However, the deformations of the adhesive and adherends create stress gradients at both ends of the overlap. So, the major part of the load transfer is mainly ensured by a small length of the overlap. In the case of dissimilar adherends, the stress gradients are asymmetric too. The effect can be reduced by using a variable-property adhesive. By varying the adhesive stiffness along the overlap, the stress distribution is modified in the joint **[4-8]**. Such joints are called functionally graded adhesive (FGA) joints. The use of a FGA tends to a homogenisation of the adhesive stress along the overlap. The use of FGA joints increased **[9-10]** offering opportunities to optimize adhesively bonded structures. The Finite Element (FE) method is an existing stress analysis method able to predict the behaviour of FGA joints **[11]**. However, due to the very high ratio between the adherend thickness and the adhesive thickness, the FE method is time costly. So to take full advantage of this technology, dedicated simulation tools need to be developed to increase the design efficiency in pre-sizing stages. 1D-bar stress analysis of FGA joints has been presented by Carbas et al. in 2014 **[5]**. Based on Volkersen's 1D-bar-homogeneous-adhesive (HA) model, the FGA is introduced. The ordinary differential equations (ODE) of the model are nonlinear due to the variable shear modulus along the overlap. To solve the problem, Carbas et al. presented a resolution scheme based on Taylor expansion in power series (TEPS). The method can be applied to a half of the overlap length and for a symmetric bilinear FGA. Later, in 2016, Stein et al. published a sandwich-type-1D-beam analysis also using TEPS in their resolution. Their model works for any gradation of the adhesive properties and is suitable for unbalanced joints **[12-13]**. Finally, in 2018, the second

author of the present paper worked on an analysis of a FGA joint under a combined thermal and mechanical load **[7]**. The equations are solved through the ME technique **[14]** and through TEPS in 1D-bar analysis. Only the ME technique was used in 1D-beam analysis. The ME is a 4-node brick gathering the adherends and the adhesive layer in one single element. The FGA joint analysis is performed thanks to a mesh of MEs along the overlap to take account of the variations of the adhesive modulus. The aim of this paper is to present an approached method to formulate a unique ME, for a whole bonded overlap involving graduation of the adhesive properties. Firstly, the approached method is explained for a 1D-bar framework with homogeneous-adhesive (HA) and graded properties. Then, part 2, the same method is used to develop an HA ME and a FGA ME with a 1D beam model. Finally, part 3, the results are compared to a FE model published in **[15]**. Moreover, the stiffness matrices, in the homogeneous cases, are compared with the exact stiffness matrices developed in **[14]**.

The configuration used for comparison is the same one as in **[15]** and is shown in Figure 1. The numerical values, of the problem parameters, are detailed later, in Table 1.

Finally, the MATLAB codes, used to get the results presented in this paper, are available as a supplementary material.

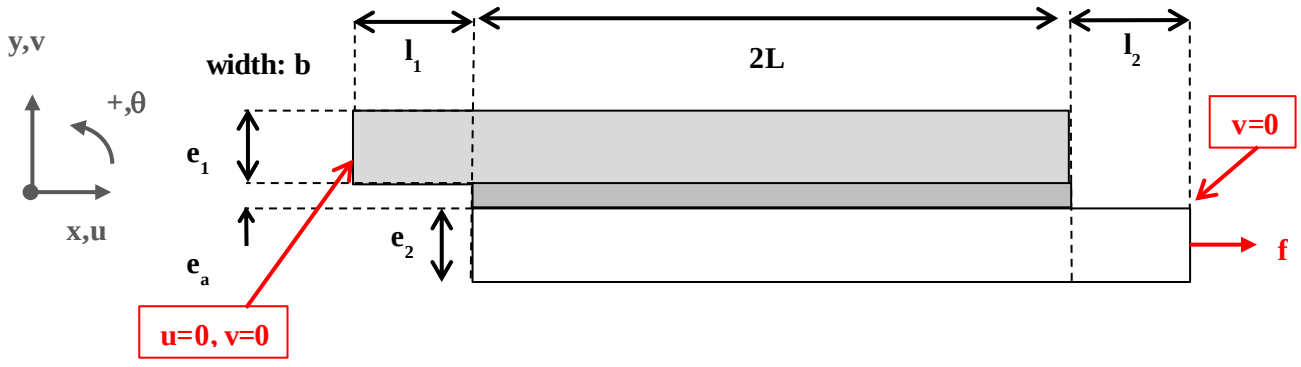


Figure 1: Simply supported single-lap involving the geometrical parameters, boundary conditions and in-plane loading.

2. Development of the approached stiffness matrix of a 1D-bar macro-element

2.1 Introduction to the macro-element technique

The ME technique is inspired by the FE method as the structure is discretized and the nodes of the ME are linked through a stiffness matrix. However, the shape functions are not assumed but derived directly from the governing equations of the system. Thus, the predicted distribution of the displacements and internal forces in the adherends, along the overlap, does not depend on a mesh density. Then, a single ME is enough to represent a whole bonded overlap.

Once the global stiffness matrix [K] of the complete structure is computed, the resolution of the system [K] $U_e = F_e$ gives the nodal displacements U_e of the joints as a function of the vector of the nodal forces F_e . Then, the stresses in the adhesive and in the adherends are computed from the constitutive equations and the nodal displacements.

The development of the ME is highly dependent on the simplifying assumptions made. The exact expression for the stiffness matrix is obtained if the ODEs system can be solved by hand. This paper is focused on a FGA joint, thus the properties of the adhesive are not constant along the overlap. The choice is made to use an approached method to solve the ODEs system and so, to derive an approached stiffness matrix for the whole bonded overlap joint. As did Hart-Smith in his paper **[16]** to find the shear stress in a scarfed bonded overlap and Carbas to study a FGA joint **[5]**, approximations of the solutions of the ODEs are done with TEPS.

2.2 Assumptions and governing equations

The development of the 1D-bar ME is based on the following assumptions:

(i) both adherends are modelled as bars made of a homogeneous linear elastic material;

(ii) the adhesive layer is modelled as an infinite number of shear springs linking the upper and lower adherends;

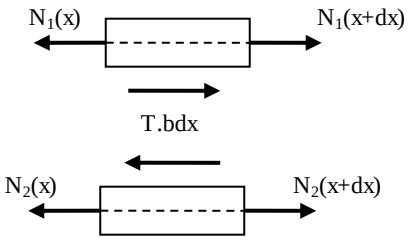
(iii) the adhesive thickness is constant along the overlap;

(iv) the adhesive stress is constant in the adhesive thickness.

The same equilibrium as Volkersen's **[17]** is used here (see Figure 2). For both adherends, it leads to:

$$\frac{dN_p(x)}{dx} = (-1)^p bT(x) \quad , \quad p = 1,2 \qquad \textbf{(1)}$$

where N_p is the normal force of the adherend p, T the adhesive shear stress and b the overlap width.



The normal force N_p in each adherend is equal to:

$$N_p(x) = A_p \frac{du_p(x)}{dx} \quad , \qquad p = 1,2 \qquad \textbf{(2)}$$

where $A_p = E_p e_p b$ is the membrane stiffness of the adherend p, with E_p and e_p the Young's Modulus and the thickness of the adherend p. The normal displacement u_p is the displacement of the point on the neutral line of the adherend p at the abscissa x.

The expression for the shear stress in the adhesive layer depends on the expression for its shear modulus. The first case considered is a joint with HA properties.

2.3 *Homogeneous adhesive macro-element (HA ME)*

The constitutive equation of the adhesive layer reads:

$$T(x) = \frac{G_a}{e_a}\left(u_2(x) - u_1(x)\right) \quad \textbf{(3)}$$

where G_a is the shear modulus of the adhesive and e_a the thickness of the adhesive layer. By combining equations (1), (2) and (3), the equilibrium for each adherend becomes:

$$E_p e_p \frac{d^2 u_p(x)}{dx^2} = (-1)^p \frac{G_a}{e_a}\left(u_2(x) - u_1(x)\right) \quad , \quad p = 1,2 \quad \textbf{(4)}$$

The solution functions u_1 and u_2 are searched as TEPS for any *x* between -*L* and *L*:

$$u_p(x) = \sum_{n=0}^{+\infty} u_{p_n} x^n \quad , \quad p = 1,2 \quad ; \quad x \in [-L, L] \quad \textbf{(5)}$$

The unknowns now become the parameters of the series say u_{p_n}. The following variable change is made:

$$\zeta = \frac{x}{L} \quad \textbf{(6)}$$

By changing the variable x in equation (5), the solution is searched for any ζ between -1 and 1.

$$u_p(x) = \sum_{n=0}^{+\infty} u_{p_n} (\zeta L)^n = \sum_{n=0}^{+\infty} u_{p_n} L^n \zeta^n = \sum_{n=0}^{+\infty} \left(u_p\right)_n \zeta^n \quad , \quad p = 1,2 \quad ; \quad \zeta \in [-1,1] \quad \textbf{(7)}$$

with the following notation set:

$$\forall\, n, \left(u_p\right)_n = u_{p_n} L^n \quad , \quad p = 1,2 \quad \textbf{(8)}$$

The m^{th} derivatives of u_p is:

$$\frac{d^m u_p(x)}{dx^m} = \frac{1}{L^m}\frac{d^m u_p(\zeta)}{d\zeta^m} = \frac{1}{L^m}\sum_{n=0}^{+\infty} \frac{(n+m)!}{n!} \left(u_p\right)_{n+m} \zeta^n \quad , \quad p = 1,2 \quad ; \quad \zeta \in [-1,1] \quad \textbf{(9)}$$

The expressions for u_1 and u_2 are replaced in equation (4):

$$E_p e_p \frac{1}{L^2} \sum_{n=0}^{+\infty} \frac{(n+2)!}{n!} \left(u_p\right)_{n+2} \zeta^n$$
$$= (-1)^p \frac{G_a}{e_a} \left(\sum_{n=0}^{+\infty} (u_2)_n \zeta^n - \sum_{n=0}^{+\infty} (u_1)_n \zeta^n \right) \quad , \quad p = 1,2 \tag{10}$$

Then, for any n, there are two second-order recursive equations:

$$\forall n \ , \quad E_p e_p \frac{1}{L^2} \frac{(n+2)!}{n!} \left(u_p\right)_{n+2} = (-1)^p \frac{G_a}{e_a} ((u_2)_n - (u_1)_n) \quad , \quad p = 1,2 \tag{11}$$

To solve numerically this problem, both series are truncated at the maximum order $N_u - 1$. So N_u is the total number of terms in each series u_p.The vector of the unknown parameters is:

$$U_T = \begin{pmatrix} (u_1)_0 \\ (u_1)_1 \\ \vdots \\ (u_1)_{N_u-1} \\ (u_2)_0 \\ (u_2)_1 \\ \vdots \\ (u_2)_{N_u-1} \end{pmatrix} \tag{12}$$

So, U_T is a $2N_u$-long vector.

As equations (11) are second-order-recursive equations, each equation is considered only for $0 \leq n \leq N_u - 3$, which leads to a $2(N_u - 2)$-equation system. Four more equations are required to solve the system. So, the nodal displacement boundary conditions are added:

$$\begin{cases} u_1(\zeta = -1) = \sum_{n=0}^{N_u-1} (u_1)_n (-1)^n = u_i \\ u_2(\zeta = -1) = \sum_{n=0}^{N_u-1} (u_2)_n (-1)^n = u_j \\ u_1(\zeta = 1) = \sum_{n=0}^{N_u-1} (u_1)_n (1)^n = u_k \\ u_2(\zeta = 1) = \sum_{n=0}^{N_u-1} (u_2)_n (1)^n = u_l \end{cases} \tag{13}$$

The global system of linear equations is written in matrix form as follows:

$$D_T U_T = \begin{pmatrix} [0]_{2(N_u-2)} \\ u_i \\ u_j \\ u_k \\ u_l \end{pmatrix} \quad \textbf{(14)}$$

where D_T is the $2N_u$ square matrix of the system including the nodal displacement boundary conditions and U_T is the vector of the unknown parameters of the truncated series. $[0]_{2(N_u-2)}$ is the $2(N_u-2)$-long null vector coming from the system derived from equation (11). By knowing the nodal displacements, the displacement at each point of the overlap can be computed, as the normal force thanks to equation (2).

However, the objective is to build the stiffness matrix of the ME. The way to obtain it is the following. The nodal force boundary conditions are written according to the sign convention defined Figure 3:

$$\begin{cases} N_1(\zeta=-1) = -\dfrac{A_1}{L}\displaystyle\sum_{n=0}^{N_u-1}(n+1)(u_1)_{n+1}(-1)^n = Q_i \\ N_2(\zeta=-1) = -\dfrac{A_2}{L}\displaystyle\sum_{n=0}^{N_u-1}(n+1)(u_2)_{n+1}(-1)^n = Q_j \\ N_1(\zeta=1) = \dfrac{A_1}{L}\displaystyle\sum_{n=0}^{N_u-1}(n+1)(u_1)_{n+1}(1)^n = Q_k \\ N_2(\zeta=1) = \dfrac{A_2}{L}\displaystyle\sum_{n=0}^{N_u-1}(n+1)(u_2)_{n+1}(1)^n = Q_l \end{cases} \quad \textbf{(15)}$$

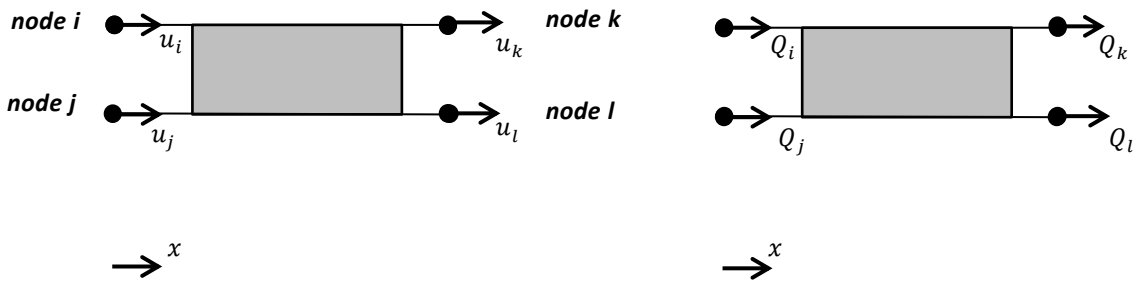


Figure 3: Nodal boundary condition diagram, 1D-bar kinematics. Nodal displacement (force) sign convention on the right (left) hand-side.

The boundary conditions are written in matrix form with the same size as the previous system:

$$L_T U_T = \begin{pmatrix} Q_i \\ Q_j \\ Q_k \\ Q_l \end{pmatrix} \quad \textbf{(16)}$$

where L_T is the $4 * 2N_u$ rectangular matrix representing the equation (15) and U_T is the vector of the unknown parameters of the truncated series. The vector of the unknowns is expressed from equation (14):

$$U_T = D_T^{-1} \begin{pmatrix} [0]_{2(N_u-2)} \\ u_i \\ u_j \\ u_k \\ u_l \end{pmatrix} \quad \textbf{(17)}$$

Finally, the nodal displacements are linked to the nodal forces by combining equations (16) and (17):

$$L_T D_T^{-1} \begin{pmatrix} [0]_{2(N_u-2)} \\ u_i \\ u_j \\ u_k \\ u_l \end{pmatrix} = \begin{pmatrix} Q_i \\ Q_j \\ Q_k \\ Q_l \end{pmatrix} \quad \textbf{(18)}$$

From equation (17), the stiffness matrix of the joint is the $4 * 4$ square matrix:

$$K_{BBa} = [L_T D_T^{-1}]_{\substack{2N_u-4\ldots 2N_u \\ 2N_u-4\ldots 2N_u}} \quad \textbf{(19)}$$

Thanks to numerical tests, it is interesting to notice the stiffness matrix K_{BBa} has always been symmetric.

2.4 Functionally graded adhesive macro-element (FGA ME)

The case of a FGA joint is now considered. The variations of the stiffness of the adhesive along the overlap are described as a TEPS with known parameters.

$$G_a(x) = \sum_{n=0}^{+\infty} G_{a_n} x^n \quad , \quad ; \quad x \in [-L, L] \quad \textbf{(20)}$$

As in the previous part, the same variable change is made:

$$G_a(\zeta) = \sum_{n=0}^{+\infty} (G_a)_n \zeta^n \quad , \quad ; \quad \zeta \in [-1,1] \quad \textbf{(21)}$$

Where, $(G_a)_n = L^n G_{a_n}$. Due to a non-homogeneous stiffness along the overlap, the constitutive equation of the adhesive layer is:

$$T(\zeta) = \frac{G_a(\zeta)}{e_a}\left(u_2(\zeta) - u_1(\zeta)\right) \quad \textbf{(22)}$$

The equilibrium equations (4) read now, for each adherend p:

$$E_p e_p \frac{1}{L^2}\sum_{n=0}^{+\infty}\frac{(n+2)!}{n!}\left(u_p\right)_{n+2}\zeta^n = (-1)^p \frac{1}{e_a}\sum_{n=0}^{+\infty}(G_a)_n\zeta^n\left(\sum_{n=0}^{+\infty}(u_2)_n\zeta^n - \sum_{n=0}^{+\infty}(u_1)_n\zeta^n\right) \quad \textbf{(23)}$$

$p = 1,2$

Thanks to the Cauchy product, the equations become:

$$E_p e_p \frac{1}{L^2}\sum_{n=0}^{+\infty}\frac{(n+2)!}{n!}\left(u_p\right)_{n+2}\zeta^n = (-1)^p \frac{1}{e_a}\left(\sum_{n=0}^{+\infty}\sum_{k=0}^{n}(G_a)_{n-k}(u_2)_k\zeta^n - \sum_{n=0}^{+\infty}\sum_{k=0}^{n}(G_a)_{n-k}(u_1)_k\zeta^n\right) \quad \textbf{(24)}$$

$p = 1,2$

So the recursive equations have two sums due to the series products:

$$\forall\, n\,, \quad E_p e_p \frac{1}{L^2}\frac{(n+2)!}{n!}\left(u_p\right)_{n+2} = (-1)^p \frac{1}{e_a}\left(\sum_{k=0}^{n}(G_a)_{n-k}(u_2)_k - \sum_{k=0}^{n}(G_a)_{n-k}\quad(u_1)_k\right) \quad \textbf{(25)}$$

$p = 1,2$

Then, with the same method as before, the stiffness matrix of the FGA ME is obtained. Equations (25) replace equations (11) to derive the $2(N_u - 2)$ first lines of the matrix D_T. The same nodal-boundary conditions (13) are used to complete the matrix D_T, while equations (15) are used to derive the L_T matrix. Finally, notice the truncation of the adhesive shear modulus serie is the same as the displacement series. More terms in the shear modulus series, more terms in the displacement series are required.

3. Development of the approached stiffness matrix of a 1D-beam macro-element

3.1 Assumptions, governing equations and parameterization

The development of the 1D-beam ME is based on the following assumptions:

(i) both adherends are modelled as linear elastic Euler-Bernoulli laminated beams ;

(ii) the adhesive layer is modelled as an infinite number of shear springs and peel springs linking the upper and lower adherends;

(iii) the adhesive thickness is constant along the overlap;

(iv) the adhesive stresses are constant in the adhesive thickness.

The equilibrium of the joint (see Figure 4) comes from Goland and Reissner's analysis **[18]**. The system of equilibrium equations is:

$$\begin{cases} \frac{dN_p}{dx} = (-1)^p bT \\ \frac{dV_p}{dx} = (-1)^{p+1} bS \\ \frac{dM_p}{dx} + V_p + \frac{be_p}{2} T = 0 \end{cases} \quad , \quad p = 1,2 \qquad \textbf{(26)}$$

where N_p is the normal force of the adherend p, V_p its shear force and M_p its bending moment at the abscissa x. T is the adhesive shear stress and S is the adhesive peel stress of the adhesive layer. b is the overlap width.

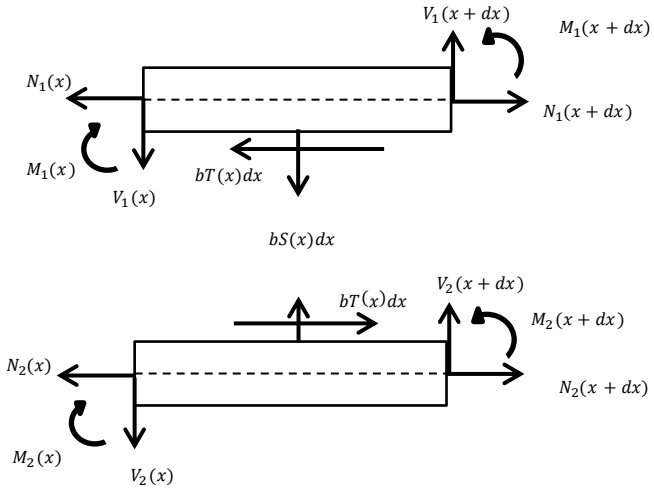


Figure 4: Free body diagram of infinitesimal pieces included between x and $x+dx$ of both adherends in the overlap region under 1D-beam kinematics. Subscript 1 (2) refers to the upper (lower) adherend.

The constitutive equations of the adherends are:

$$\begin{cases} N_p(x) = A_p \frac{du_p(x)}{dx} - B_p \frac{d\theta_p(x)}{dx} \\ M_p(x) = -B_p \frac{du_p(x)}{dx} + D_p \frac{d\theta_p(x)}{dx} \\ \theta_p(x) = \frac{dv_p(x)}{dx} \end{cases} \quad , \quad p = 1,2 \qquad \textbf{(27)}$$

where A_p is the membrane stiffness of the adherend p, B_p its coupling membrane-bending stiffness, D_p its bending stiffness and θ_p its bending angle. By differentiating the third relation in equation (26), and replacing the expression for V_p, the system becomes:

$$\begin{cases} \frac{dN_p(x)}{dx} = (-1)^p bT(x) \\ \frac{d^2M_p(x)}{dx^2} + (-1)^{p+1} bS(x) + \frac{be_p}{2}\frac{dT(x)}{dx} = 0 \end{cases} \quad , \quad p = 1,2 \qquad \textbf{(28)}$$

To go further in the analysis, as before, the first case considered is an adhesive layer with homogeneous stiffness properties. Then the case with graded properties is treated.

3.2 Homogeneous adhesive macro-element (HA ME)

In this first case, the constitutive equations of the adhesive layer are:

$$\begin{cases} T = \frac{G_a}{e_a}\left(u_2 - u_1 - \frac{e_2}{2}\theta_2 - \frac{e_1}{2}\theta_1\right) \\ S = -\frac{E_a}{e_a}(v_2 - v_1) \end{cases} \qquad \textbf{(29)}$$

The adhesive peel modulus E_a of the adhesive layer is now introduced. Please notice that the adhesive peel modulus is the parameter characterising the transverse tensile behaviour of the adhesive layer. According to modelling choices of the adhesive layer, the adhesive peel modulus can be the adhesive Young's modulus or the effective peel modulus of the adhesive layer [19] [20] [21] [22]. These modelling choices will not be discussed in the present paper.

By replacing in equation (28) the expression for T and S from equation (29), the system becomes:

$$\begin{cases} A_p\frac{d^2u_p}{dx^2} - B_p\frac{d^2\theta_p}{dx^2} + (-1)^{p+1} b\frac{G_a}{e_a}\left(u_2 - u_1 - \frac{e_2}{2}\theta_2 - \frac{e_1}{2}\theta_1\right) = 0 \\ \frac{d^2}{dx^2}\left(-B_p\frac{du_p}{dx} + D_p\frac{d\theta_p}{dx}\right) + (-1)^p b\frac{E_a}{e_a}(v_2 - v_1) + \frac{be_pG_a}{2e_a}\frac{d}{dx}\left(u_2 - u_1 - \frac{e_2}{2}\theta_2 - \frac{e_1}{2}\theta_1\right) = 0 \end{cases} \qquad \textbf{(30)}$$

$p = 1,2$

$$\begin{cases} A_p \dfrac{d^2u_p}{dx^2} - B_p \dfrac{d^3v_p}{dx^3} + (-1)^{p+1} b \dfrac{G_a}{e_a}\left(u_2 - u_1 - \dfrac{e_2}{2}\dfrac{dv_2}{dx} - \dfrac{e_1}{2}\dfrac{dv_1}{dx}\right) = 0 \\ \left(-B_p \dfrac{d^3u_p}{dx^3} + D_p \dfrac{d^4v_p}{dx^4}\right) + (-1)^p b \dfrac{E_a}{e_a}(v_2 - v_1) + \dfrac{be_p}{2}\dfrac{G_a}{e_a}\left(\dfrac{du_2}{dx} - \dfrac{du_1}{dx} - \dfrac{e_2}{2}\dfrac{d^2v_2}{dx^2} - \dfrac{e_1}{2}\dfrac{d^2v_1}{dx^2}\right) = 0 \end{cases} \quad \textbf{(31)}$$

$p = 1,2$

The solution functions u_1, u_2, v_1, v_2 are expressed as TEPS:

$$\begin{cases} u_p(x) = \sum_{n=0}^{+\infty} {u_p}_n x^n \quad , \quad p = 1,2 \quad ; \quad x \in [-L, L] \\ v_p(x) = \sum_{n=0}^{+\infty} {v_p}_n x^n \quad , \quad p = 1,2 \quad ; \quad x \in [-L, L] \end{cases} \quad \textbf{(32)}$$

And, with the same variable change as in part 2, it reads:

$$\begin{cases} u_p(\zeta) = \sum_{n=0}^{+\infty} \left(u_p\right)_n \zeta^n \quad , \quad p = 1,2 \quad ; \quad \zeta \in [-1,1] \\ v_p(\zeta) = \sum_{n=0}^{+\infty} \left(v_p\right)_n \zeta^n \quad , \quad p = 1,2 \quad ; \quad \zeta \in [-1,1] \end{cases} \quad \textbf{(33)}$$

with:

$$\begin{cases} \forall\, n, \quad \left(u_p\right)_n = {u_p}_n L^n \quad , \quad p = 1,2 \\ \forall\, n, \quad \left(v_p\right)_n = {v_p}_n L^n \quad , \quad p = 1,2 \end{cases} \quad \textbf{(34)}$$

The expression for u_1, u_2, v_1 and v_2 are replaced in equation (31):

$$\begin{cases} \dfrac{A_p}{L^2}\sum_{n=0}^{+\infty}\left(\dfrac{(n+2)!}{n!}\left(u_p\right)_{n+2}\right)\zeta^n - \dfrac{B_p}{L^3}\sum_{n=0}^{+\infty}\left(\dfrac{(n+3)!}{n!}\left(v_p\right)_{n+3}\right)\zeta^n \\ \quad + (-1)^{p+1} b \dfrac{G_a}{e_a}\left(\sum_{n=0}^{+\infty}\left((u_2)_n - (u_1)_n - \dfrac{e_2}{2L}\dfrac{(n+1)!}{n!}(v_2)_{n+1} - \dfrac{e_1}{2L}\dfrac{(n+1)!}{n!}(v_1)_{n+1}\right)\zeta^n\right) = 0 \\ \\ -\dfrac{B_p}{L^3}\sum_{n=0}^{+\infty}\left(\dfrac{(n+3)!}{n!}\left(u_p\right)_{n+3}\right)\zeta^n + \dfrac{D_p}{L^4}\sum_{n=0}^{+\infty}\left(\dfrac{(n+4)!}{n!}\left(v_p\right)_{n+4}\right)\zeta^n + (-1)^p b \dfrac{E_a}{e_a}\sum_{n=0}^{+\infty}\left((v_2)_n - (v_1)_n\right)\zeta^n \\ + \dfrac{be_p}{2}\dfrac{G_a}{e_a}\left(\sum_{n=0}^{+\infty}\left(\dfrac{1}{L}\dfrac{(n+1)!}{n!}(u_2)_{n+1} - \dfrac{1}{L}\dfrac{(n+1)!}{n!}(u_1)_{n+1} - \dfrac{e_2}{2L^2}\dfrac{(n+2)!}{n!}(v_2)_{n+2} - \dfrac{e_1}{2L^2}\dfrac{(n+2)!}{n!}(v_1)_{n+2}\right)\zeta^n\right) = 0 \end{cases} \quad \textbf{(35)}$$

$p = 1,2$

The recursive equations of the system are:

$$\forall n,\begin{cases} \frac{A_p}{L^2}\frac{(n+2)!}{n!}\left(u_p\right)_{n+2}-\frac{B_p}{L^3}\frac{(n+3)!}{n!}\left(v_p\right)_{n+3} \\ +(-1)^{p+1}b\frac{G_a}{e_a}\left(\left(u_2\right)_n-\left(u_1\right)_n-\frac{e_2}{2L}\frac{(n+1)!}{n!}\left(v_2\right)_{n+1}-\frac{e_1}{2L}\frac{(n+1)!}{n!}\left(v_1\right)_{n+1}\right)=0 \\ \\ -\frac{B_p}{L^3}\left(\frac{(n+3)!}{n!}\left(u_p\right)_{n+3}\right)+\frac{D_p}{L^4}\left(\frac{(n+4)!}{n!}\left(v_p\right)_{n+4}\right)+(-1)^p b\frac{E_a}{e_a}\left(\left(v_2\right)_n-\left(v_1\right)_n\right) \\ +\frac{be_p}{2}\frac{G_a}{e_a}\left(\frac{1}{L}\frac{(n+1)!}{n!}\left(u_2\right)_{n+1}-\frac{1}{L}\frac{(n+1)!}{n!}\left(u_1\right)_{n+1}-\frac{e_2}{2L^2}\frac{(n+2)!}{n!}\left(v_2\right)_{n+2}-\frac{e_1}{2L^2}\frac{(n+2)!}{n!}\left(v_1\right)_{n+2}\right)=0 \end{cases} \quad \textbf{(36)}$$

$p=1,2$

The first equation for each adherend is considered as a second-order recursive equation on the parameter (u_j) and the second equation is a fourth-order recursive equation on the parameter (v_j). Contrary to part 2, the truncation is defined as the maximum value that n can be. For any truncation at $n=N$, the last term of the u_j series is $(u_j)_{N+2}$ and the last term of the v_j series is $(v_j)_{N+4}$. Let be $N+2=N_u-1$ and $N+4=N_v-1$, the number of terms in the series u and v are respectively N_u and N_v. The two series have a different number of terms. Moreover, during the computation of the matrix of the system, for the last equation at $n=N$, in the second equation of (36) the term $(u_j)_{N+3}$ is set to zero as it does not exist in the frame of the truncation defined here.

Using the same method as in part 2, the nodal boundary conditions are applied to derive the stiffness matrix of the joint. The sign convention visible in Figure 5 is taken.

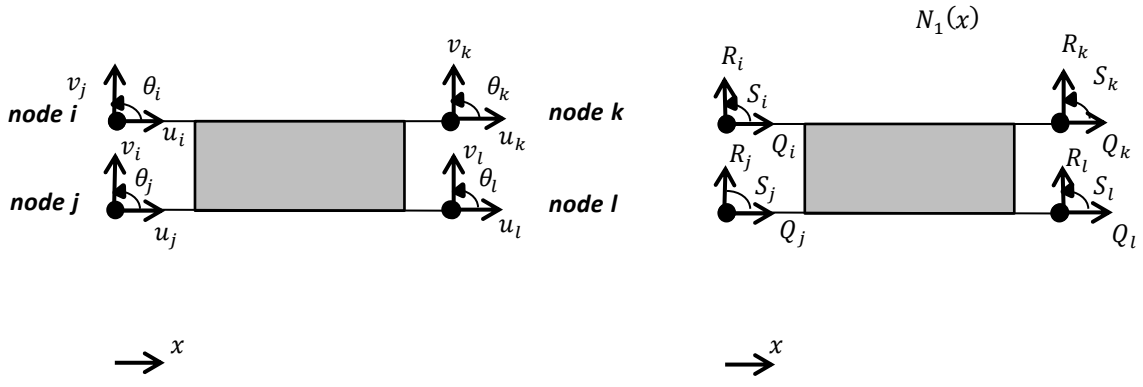


Figure 5: Nodal boundary condition diagram, 1D-beam kinematics. Nodal displacement (force) sign convention on the right (left) hand-side.

The nodal displacement boundary conditions are:

$$\begin{pmatrix} u_1(-1) \\ v_1(-1) \\ \theta_1(-1) \\ u_2(-1) \\ v_2(-1) \\ \theta_2(-1) \\ u_1(1) \\ v_1(1) \\ \theta_1(1) \\ u_2(1) \\ v_2(1) \\ \theta_2(1) \end{pmatrix} = \begin{pmatrix} u_i \\ v_i \\ \theta_i \\ u_j \\ v_j \\ \theta_j \\ u_k \\ v_k \\ \theta_k \\ u_l \\ v_l \\ \theta_l \end{pmatrix} \quad \textbf{(37)}$$

The nodal force boundary conditions are:

$$\begin{pmatrix} N_1(-1) \\ V_1(-1) \\ M_1(-1) \\ N_2(-1) \\ V_2(-1) \\ M_2(-1) \\ N_1(1) \\ V_1(1) \\ M_1(1) \\ N_2(1) \\ V_2(1) \\ M_2(1) \end{pmatrix} = \begin{pmatrix} N_i \\ R_i \\ S_i \\ N_j \\ R_j \\ S_j \\ N_k \\ R_k \\ S_k \\ N_l \\ R_l \\ S_l \end{pmatrix} \quad \textbf{(38)}$$

The expressions for V_1 and V_2 come from the moment equilibrium equation (26). The stiffness matrix is defined as in part 2. The matrix D_T and L_T are written thanks to the equations (36), (37) and (38).

Thus, for any truncation at n=N, a $12 * 12$ stiffness matrix for the 1D-beam ME is obtained with the same method.

$$K_{BBe} = [L_T D_T^{-1}]_{\substack{(2N_u+2N_v)-12 \dots (2N_u+2N_v) \\ (2N_u+2N_v)-12 \dots (2N_u+2N_v)}} \quad \textbf{(39)}$$

3.3 Functionally graded adhesive macro-element (FGA ME)

The development of the graded 1D-beam ME uses the same approach as in the 1D-bar case. The variable shear modulus and variable peel modulus of the adhesive layer are written as follow:

$$\begin{cases} G_a(x) = \sum_{n=0}^{+\infty} G_{a_n} x^n \\ E_a(x) = \sum_{n=0}^{+\infty} E_{a_n} x^n \end{cases} \quad , \quad ; \quad x \in [-L, L] \qquad \textbf{(40)}$$

The derivative of the moment equilibrium equation is modified as the shear modulus and the peel modulus are now x dependent.

The same variable change is made:

$$\begin{cases} G_a(\zeta) = \sum_{n=0}^{+\infty} (G_a)_n \zeta^n \quad ; \quad \zeta \in [-1,1] \\ E_a(\zeta) = \sum_{n=0}^{+\infty} (E_a)_n \zeta^n \quad ; \quad \zeta \in [-1,1] \end{cases} \qquad \textbf{(41)}$$

The system coming from the equilibrium is so different from equation (31) and is:

$$\begin{cases} A_p \frac{d^2 u_p}{dx^2} - B_p \frac{d^2 \theta_p}{dx^2} + (-1)^{p+1} b \frac{G_a}{e_a}\left(u_2 - u_1 - \frac{e_2}{2}\theta_2 - \frac{e_1}{2}\theta_1\right) = 0 \\ \frac{d^2}{dx^2}\left(-B_p \frac{du_p}{dx} + D_p \frac{d\theta_p}{dx}\right) + (-1)^p b \frac{E_a}{e_a}(v_2 - v_1) \\ + \frac{be_p}{2}\frac{1}{e_a}\left(\frac{dG_a}{dx}\right)\left(u_2 - u_1 - \frac{e_2}{2}\theta_2 - \frac{e_1}{2}\theta_1\right) + \frac{be_p}{2}\left(\frac{G_a}{e_a}\right)\frac{d}{dx}\left(u_2 - u_1 - \frac{e_2}{2}\theta_2 - \frac{e_1}{2}\theta_1\right) = 0 \end{cases} \qquad \textbf{(42)}$$

$p = 1,2$

Then the new recursive equations, replacing equations (36), are:

$$\forall n,\begin{cases} \frac{A_p}{L^2}\frac{(n+2)!}{n!}\left(u_p\right)_{n+2}-\frac{B_p}{L^3}\frac{(n+3)!}{n!}\left(v_p\right)_{n+3} \\ +(-1)^{p+1}\frac{b}{e_a}\sum_{k=0}^{n}\left(G_a\right)_{n-k}\left(\left(u_2\right)_k-\left(u_1\right)_k-\frac{e_2}{2L}\frac{(n+1)!}{n!}\left(v_2\right)_{k+1}-\frac{e_1}{2L}\frac{(n+1)!}{n!}\left(v_1\right)_{k+1}\right)=0 \\ -\frac{B_p}{L^3}\frac{(n+3)!}{n!}\left(u_p\right)_{n+3}+\frac{D_p}{L^4}\frac{(n+4)!}{n!}\left(v_p\right)_{n+4}+(-1)^p\frac{b}{e_a}\sum_{k=0}^{n}\left(\left(E_a\right)_{n-k}\right)\left(\left(v_2\right)_k-\left(v_1\right)_k\right) \\ +\frac{be_p}{2e_a}\sum_{k=0}^{n}\frac{1}{L}\frac{(n-k+1)!}{(n-k)!}\left(G_a\right)_{n-k+1}\left(\left(u_2\right)_k-\left(u_1\right)_k-\frac{e_2}{2L}\frac{(n+1)!}{n!}\left(v_2\right)_{k+1}-\frac{e_1}{2L}\frac{(n+1)!}{n!}\left(v_1\right)_{k+1}\right) \\ +\frac{be_p}{2e_a}\sum_{k=0}^{n}\left(\left(G_a\right)_{n-k}\right)\left(\frac{1}{L}\frac{(n+1)!}{n!}\left(u_2\right)_{k+1}-\frac{1}{L}\frac{(n+1)!}{n!}\left(u_1\right)_{k+1}-\frac{e_2}{2L^2}\frac{(n+2)!}{n!}\left(v_2\right)_{k+2}-\frac{e_1}{2L^2}\frac{(n+2)!}{n!}\left(v_1\right)_{k+2}\right)=0 \\ , \ p \end{cases} \quad \textbf{(43)}$$

$p = 1,2$

The stiffness matrix of the FGA ME in 1D-beam kinematics is computed as before. In the boundary conditions, the expression of the shear force V_p takes account of the gradation of G_a and E_a. The new recursive equations (43) and the nodal-displacement-boundary conditions lead to the D_T matrix. The matrix L_T is derived from the nodal-force-boundary conditions in 1D-beam kinematics. The derivation of the nodal-force-boundary conditions is detailed in Appendix A.

4. Validation

The validation of the approached ME with TEPS is done in two different ways. First of all, in the case of the HA ME, the exact stiffness matrix and the approached stiffness matrix developed here are compared terms by terms. Then, in the case of a FGA single lap joint, the stress distributions are compared to a FE model from a previous work **[15]**. The geometry and the material used to perform the tests are given in the following part. Then, the FE model set up is detailed and the validation finishes with the comparison of the stress curves obtained with both models.

4.1 Geometry and materials

The tests are made with a single-lap bonded joint, as visible in Figure 1. The choice is made to use the exact same set up as in **[15]**. Consequently, the geometry details are available in the following Table 1 and the material parameters used are described in Table 2.

Table 1: Geometrical parameters of the joint configuration

b (mm)	e_a (mm)	$e_1=e_2$ (mm)	L (mm)	$l_1=l_2$ (mm)
25	0.2	2	12.5	75

Table 2: **Material parameters of the adherends**

	Young's modulus (GPa)
Steel	$E_1 = 210$
Aluminium	$E_2 = 70$

In **[15]**, the shear and peel modulus variation along the overlap are defined as a symmetrical second order polynomial thanks to a maximum and a minimum value. For simplicity, the ratio between these maximum and minimum is equal to $2(1+\nu_a)$, where ν_a is the adhesive Poisson's ratio. The extreme values taken here are in Table 3.

Table 3: Adhesive material properties

$E_{a,max}$ (MPa)	$E_{a,min}$ (MPa)	ν_a
6500	2500	0.36

Finally, the structure is simply supported and loaded in the local axis of the lower adherend, as visible in Figure 1.

4.2 Description of the FE model

The validation of the approached ME method is based on a 1D FE model developed in **[15]**. The main parameters of the model are described below.

To be as close as possible to the modelling hypotheses of ME models, the 1D FE models are built from bar or beam elements for the adherends and spring elements for the adhesive layer. The nodes associated with bar or beam elements are located at the actual neutral line of the adherends. The nodes associated with the spring elements are located at the actual interfaces of adherends. In the 1D-beam model only, for each adherend along the overlap, rigid body elements are used to link the nodes of the neutral lines and to the nodes of the adherend interface.

The predicted adhesive stresses are expected to be dependent on the number of springs used. The convergence study leads to 500 elements for a 25mm long bonded overlap. The mesh density is then 20 elements per millimetre.

4.3 Stiffness matrix comparison

4.3.1 1D-bar ME

The exact stiffness matrix of the 1D-bar ME is used to validate the method to develop the HA ME. The coefficients of the two stiffness matrices tend to be equal when the number N_u increases. Thus, the choice is made to compute the error between the terms of the two matrices. A convergence indicator is defined in equation (44) and named "error" hereafter. The error is converging to zero with the convergence of the approached stiffness matrix. Figure 6 gives the error, computed for a number of terms N_u in each serie from $N_u = 5$ to $N_u = 25$ in each series.

$$error = \frac{\Sigma_{i,j}\left|[K_{exact}]_{i,j} - [K_{approached}]_{i,j}\right|}{\max_{i,j}\left([K_{exact}]_{i,j}\right)} \quad \textbf{(44)}$$

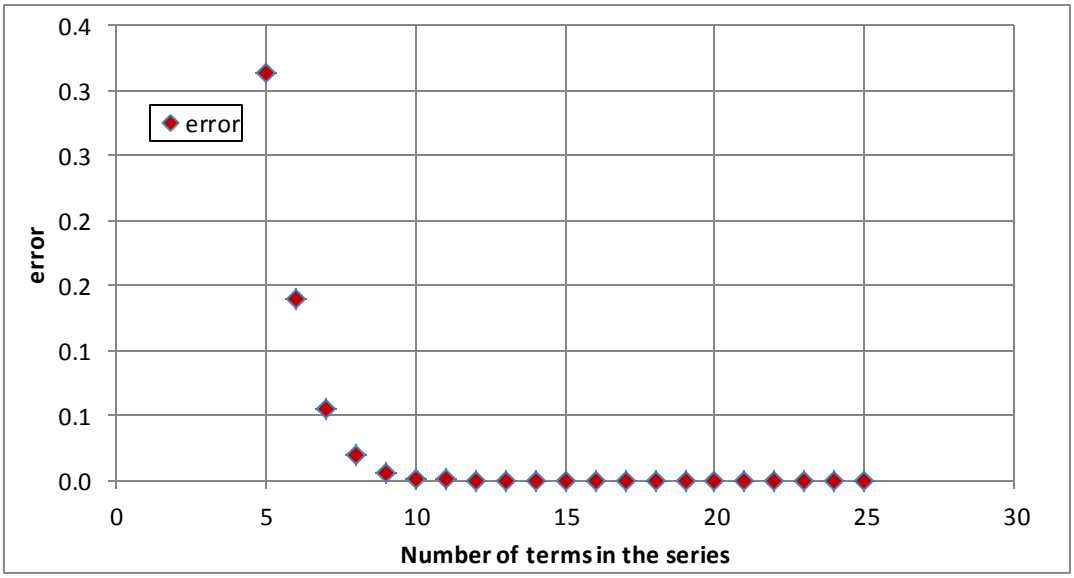


Figure 6: Evolution of the error on the stiffness matrix coefficients as a function of the number of terms in the series for 1D-bar kinematics

Figure 6 shows the error may be considered as converged for a number of terms over 10 in the series. As a result, this value is the sufficient number of terms in the series to obtain the same stress distribution in the joint as Volkersen's with the approached ME technique. Hereafter, the stress distribution obtained with different values of N_u are compared to Volkersen's solution.

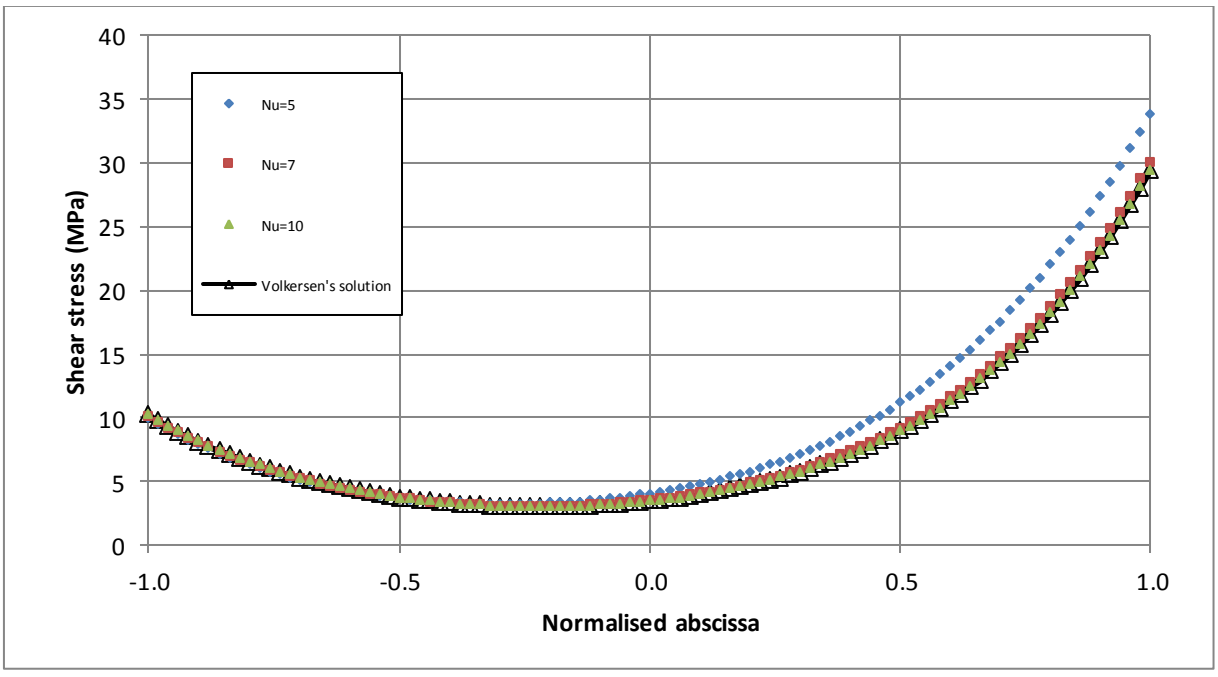


Figure 7: Evolution of the shear stress along the overlap as function of the number of terms in the series. Comparison with Volkersen's solution

The relative error at the ends of the overlap is computed from the equation (45):

$$relative\ error = \frac{ComputedValue - TargetValue}{TargetValue} \quad \textbf{(45)}$$

The $ComputedValue$ is the value given by the HA ME analysis. The $TargetValue$ is computed through Volkersen's shear stress solution. At $N_u = 10$, the order of magnitude of the maximum relative error at the ends of the overlap is 10^{-7}.

4.3.2 1D-beam ME

The stiffness matrix obtained here for a 1D-beam ME is validated with the same technique. The error is computed between the matrix developed in this work and the exact stiffness matrix. The truncation of the series is done differently. A maximum value of N is defined and the recursive equations are used N times. So, as written part 3, the sizes of the series are different between u_p and v_p. The following graph shows the error defined in equation (44) for different values of N :

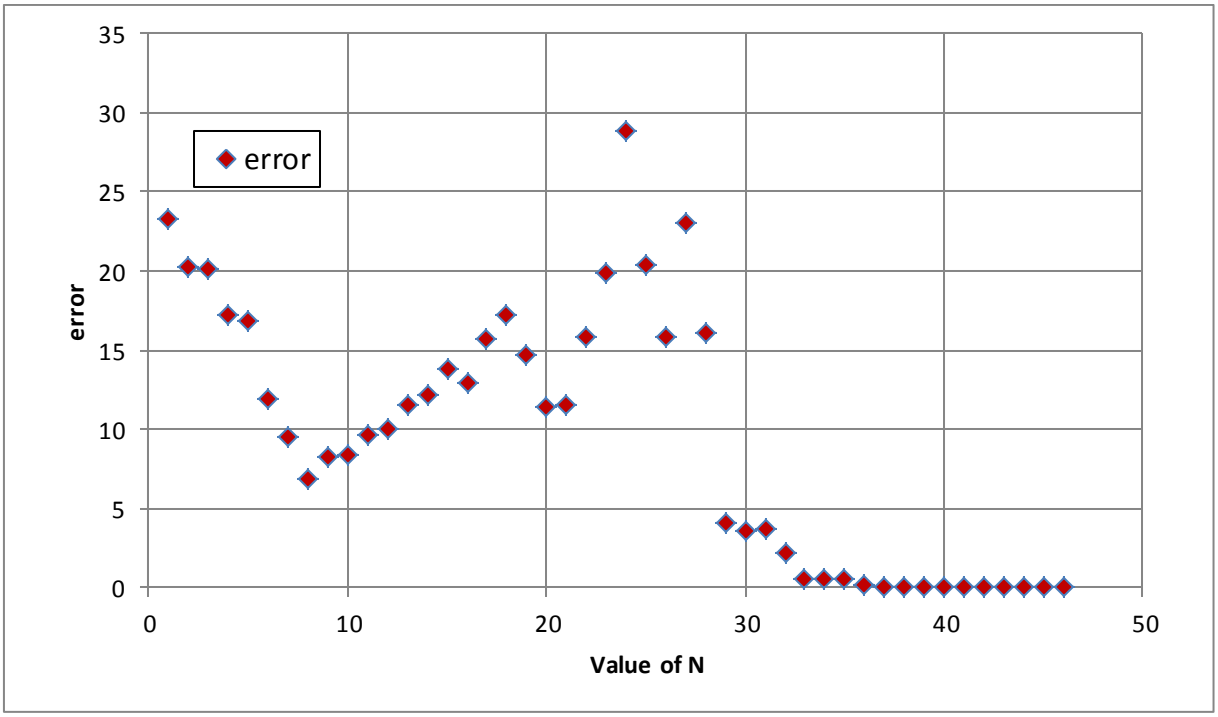
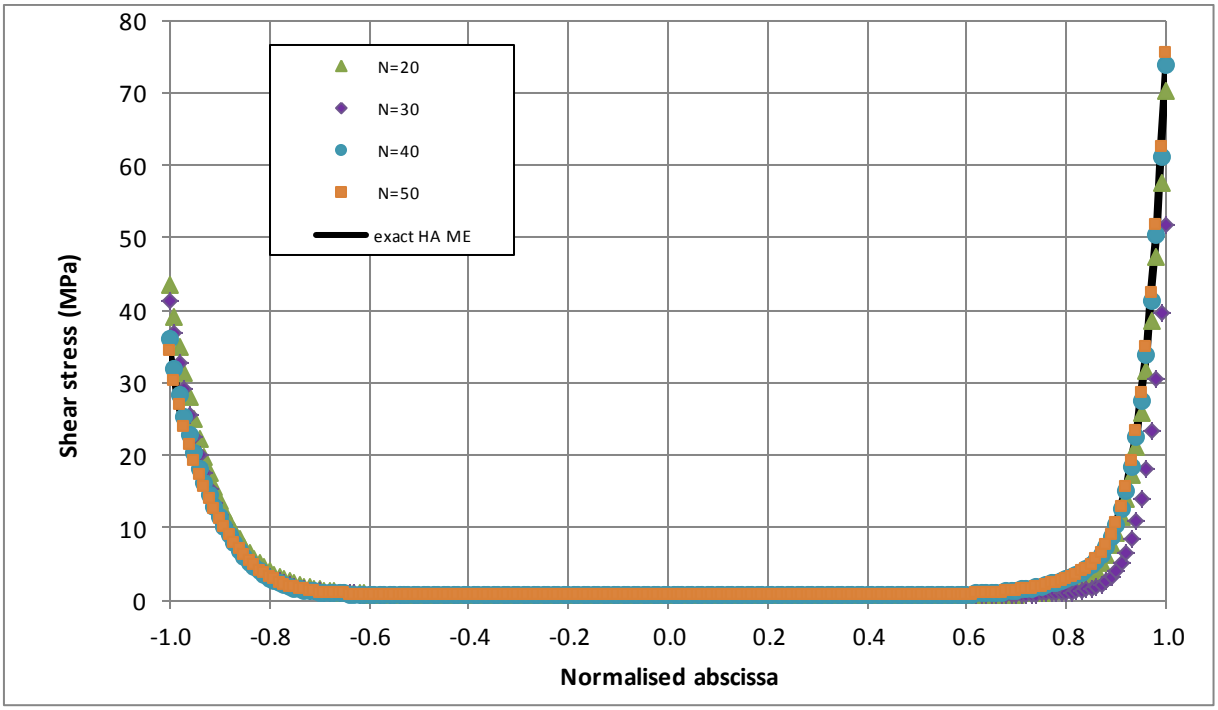
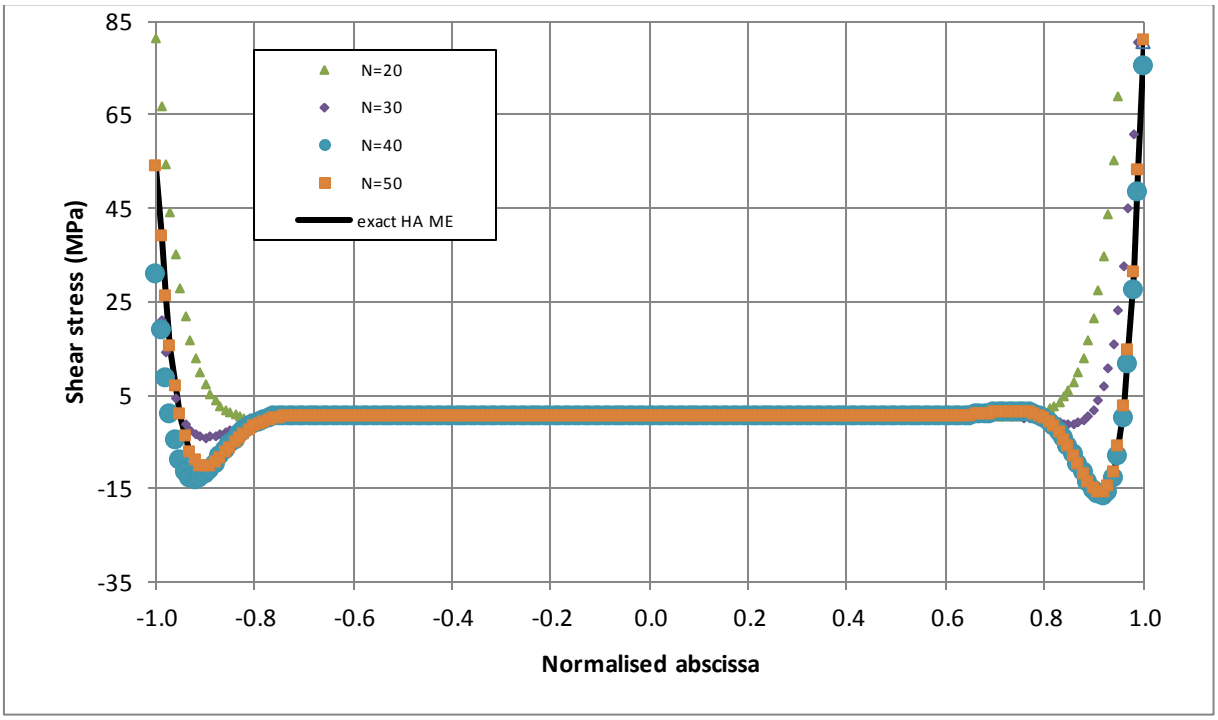


Figure 8: Evolution of the error on the stiffness matrix coefficients as function of N for 1D-beam kinematics

The approached matrix may be considered as converged for any $N \geq 40$. It means a number of terms superior to 42 for the u_p series and 44 for the v_p series. The evolution of the solutions with the values of N is plotted in Figure 9. The solution provided by an analysis performed with the exact HA ME, available in **[14]**, is used as a reference. The order of magnitude of the relative error, at both ends of the overlap, is 10^{-5} for $N \geq 40$. The relative error is computed using equation (45). The $ComputedValue$ is the value given by the HA ME analysis. The $TargetValue$ come from the analytical HA ME available in **[14]**.



a)



b)

Figure 9: Evolution, along the overlap, as a function of N for 1D-beam kinematics of a) the shear stress and b) the peel stress

Finally, in case of FGA joint, it is indicated that if the variable shear modulus and peel modulus (1D-beam kinematics only) are set up at constant along the overlap, the exact HA stiffness matrix is reached at the same number of terms in the series.

4.4 Comparison with a FE analysis of a FGA joint

This part is dedicated to the comparison between the 1D-bar and 1D-beam FE analysis, the meshed-HA ME analysis and the FGA ME analysis developed in the present paper. For all comparisons, the values of N_u and N are a little higher than in the previous HA case. The new values are: $N_u = 15$ for the 1D-bar kinematic case, and $N = 40$ for the 1D-beam kinematic case. The shear modulus and peel modulus of the adhesive vary along the overlap as a second-order polynomial with a maximum and minimum values defined Table 3.

4.4.1 1D-bar kinematic case

The solutions obtained with the FE analysis, meshed-HA ME analysis and the FGA ME analysis are plotted in Figure 10. All the analyses give similar results. The relative errors at the end of the overlap, where the stress peaks are located, are given in Table 4. As a reminder, for the FGA ME each series is 15-term long, the mesh of HA ME is made of 200 HA ME and the mesh density of the FE model is 20 elements per millimetre.

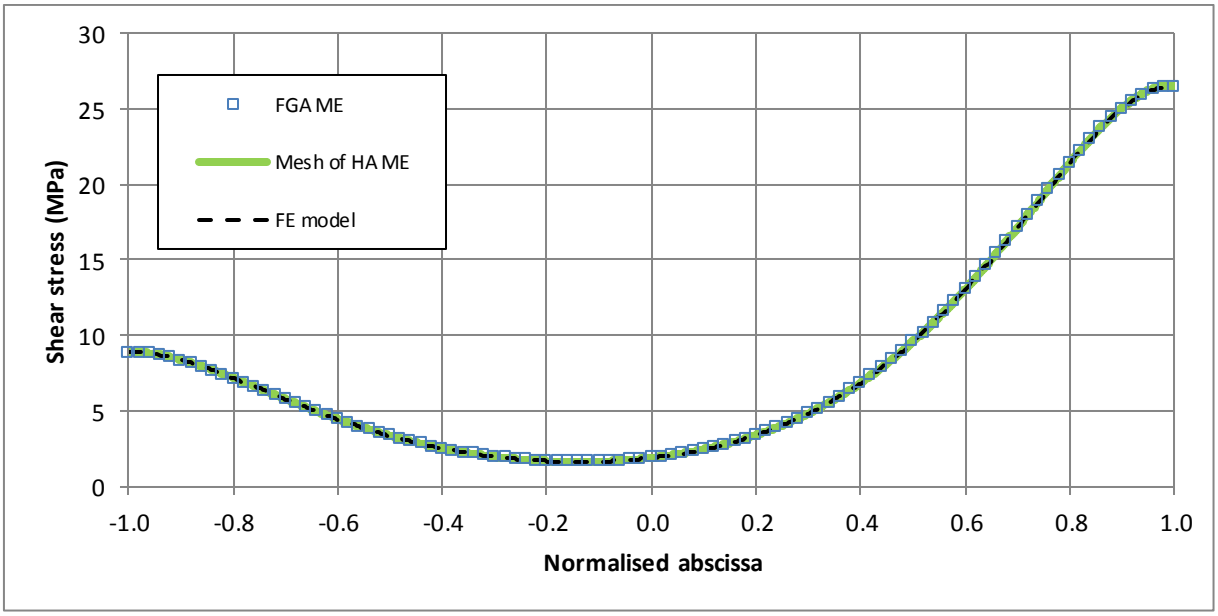


Figure 10: Comparison between the shear stress obtained thanks to a FE analysis, an analysis with a mesh of HA MEs and a FGA ME analysis for 1D-bar kinematics

Table 4: Relative shear stress relative errors at the ends of the overlap - 1D bar kinematic case

	FE model vs FGA ME
Left-hand-side shear stress peak	**-0.19%**
Righ hand-side shear stress peak	**0.10%**

The $ComputedValue$ is the value given by the FGA ME analysis. The $TargetValue$ is computed thanks to the FE analysis.

4.4.2 1D-beam kinematic case

The solutions obtained with the FE analysis, meshed-HA ME analysis and the FGA ME analysis are plotted Figure 11 (shear stress) and Figure 12 (peel stress). The relative errors at

each end of the overlap are detailed in **Table 5**. Compared to the errors available in **[15],** the approached ME method is about 10 times closer to the FE model. As a reminder, for the FGA ME the series $\boldsymbol{u_1}$ and $\boldsymbol{u_2}$ are 42-term long and the series $\boldsymbol{v_1}$ and $\boldsymbol{v_2}$ are 44-term long, the mesh of HA ME is made of 200 HA ME and the mesh density of the FE model is 20 elements per millimetre.

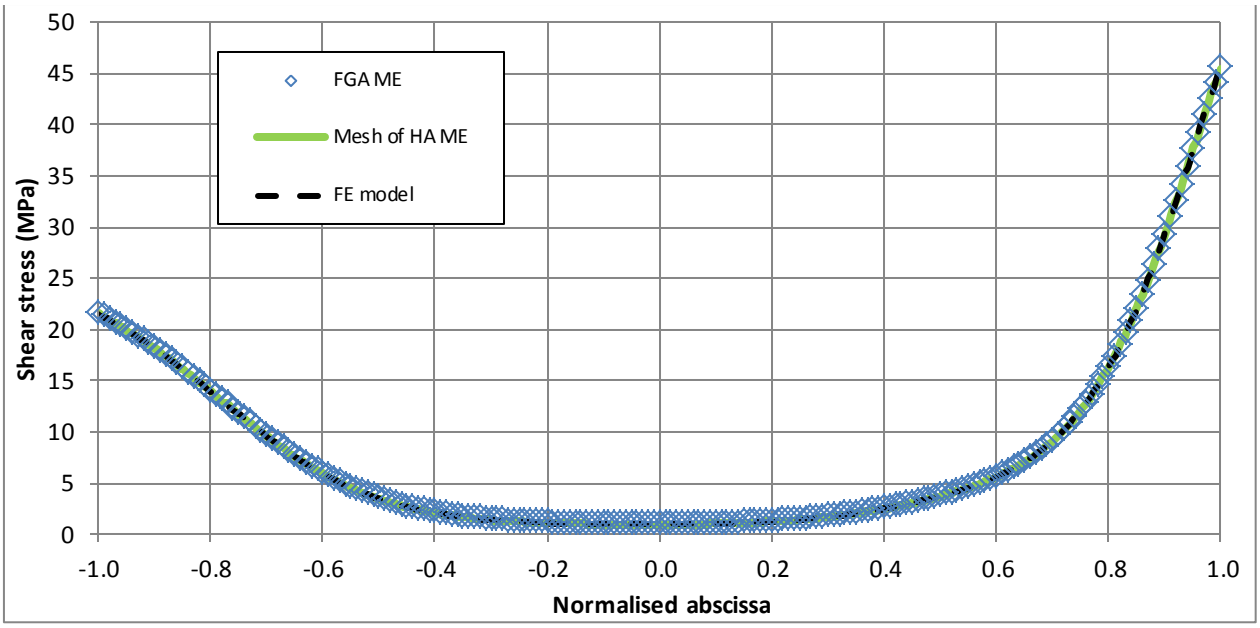


Figure 11: Comparison between the shear stress obtained by FE analysis, an analysis with a mesh of HA MEs and a FGA ME analysis for 1D-beam kinematic

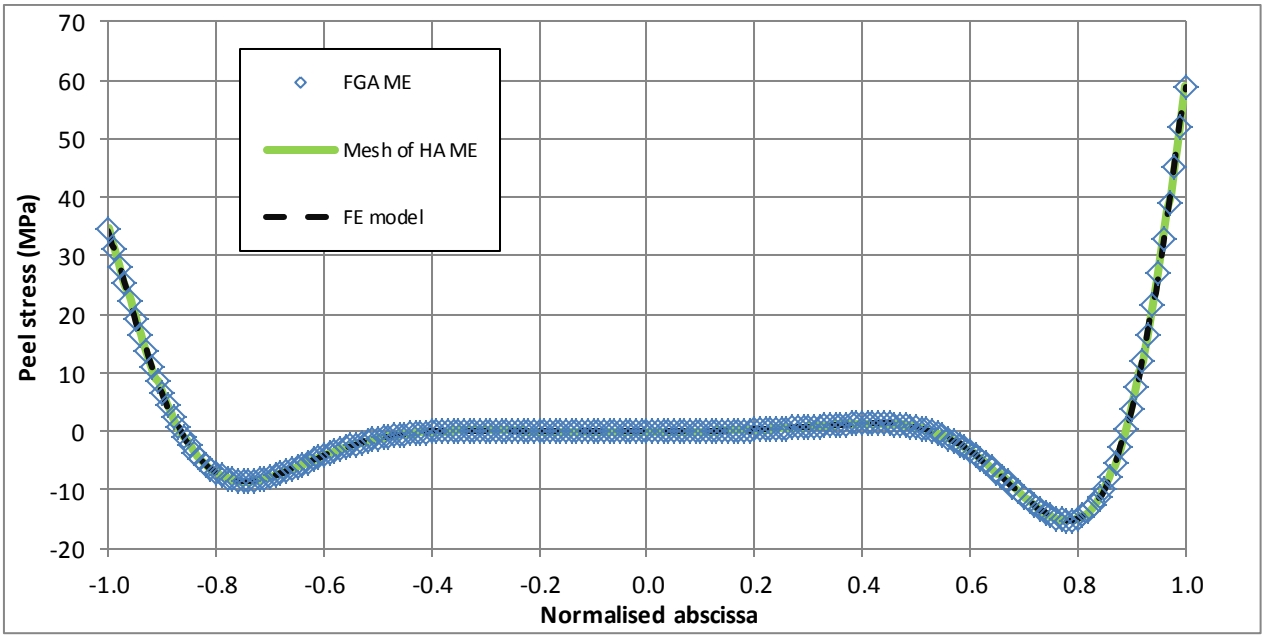


Figure 12: Comparison between the peel stress obtained by FE analysis, an analysis with a mesh of HA MEs and a FGA ME analysis for 1D-beam kinematics

Table 5: Relative shear stress and peel stress relative errors at the ends of the overlap - 1D-beam kinematic case

	FE model vs FGA ME	
	Shear Stress Ratio	**Peel Stress Ratio**
Left hand-side peak	**-0.002%**	**0.03%**
Right hand-side peak	**0.007%**	**0.03%**

5. Conclusion

In this paper, an approached method to develop ME, using TEPS, is presented. The details of the mathematical derivation are described. The results are compared to a 1D FE model and to a model using a mesh of HA ME presented in a previous work **[15]**. The models used to develop the approached ME aim to test the use of TEPS to solve differential equations. Thus Volkersen's and Goland and Reissner-based models are chosen as a first basis to test the

resolution method before applying it to more complex models. A convergence study of the approached stiffness matrix as a function of the order of the series is done in the HA case. The convergence is done with the exact expression for the stiffness matrix of a 1D-bar ME and a 1D-beam ME **[14]** as a target. A 1D-bar and 1D-beam FE models, from **[15],** are used to assess the results obtained with the approached ME of a FGA joint. Two conclusions can be made from the results. Firstly, the TEPS is a suitable tool to develop ME and solve differential equations. The exact stiffness matrix is closely approached for a reasonable number of terms in the series. Secondly, the use of TEPS to develop ME with non-homogeneous properties shows results very close to a 1D-bar and 1D-beam FE analysis. The relative error is lower than 0.01% on the shear-stress peaks and lower than 0.05% on the peel-stress peaks. The approach with a mesh of HA ME shows a higher error. This discrepancy is said to be due to the assignment strategy of the FGA modulus **[15]**. Thanks to the use of the TEPS, there is no discontinuity in the modulus values along the overlap. The solution is so less sensitive to any high-gradient variations of the modulus or stress peaks. Every continuous function can be represented by a TEPS. So the method presented here works for any FGA and a FE-equivalent solution can be computed. This work may also be used to determine the coefficients of an unknown FGA. Indeed, if the displacement field is known from experimental tests, the coefficient of the series representing the FGA can be identified. Finally, the presented method showed results very close to a FE reference solution. The truncation of the series has been defined in consequence. But the best strategy to define the truncation order in a case of a blind test still needs to be found.

Acknowledgement

The three first authors are grateful to the French institutions "Centre Technique des Industries Mécaniques" and "Direction Générale de l'Armement" for their financial support of the presented work.

Appendix A: Expression of the nodal force boundary conditions

The shear force expression comes from the third equation of (26). The derivation on the boundary condition on node i is developed. Then the final expression is given for nodes j, k and l.

From (26) and (38), the nodal force boundary conditions on node i are:

$$\begin{cases} -N_1(\zeta=-1) = -A_1\dfrac{1}{L}\dfrac{du_1(-1)}{d\zeta} + B_1\dfrac{1}{L}\dfrac{d\theta_1(-1)}{d\zeta} = Q_i \\ -V_1(\zeta=-1) = \dfrac{1}{L}\dfrac{dM_1(-1)}{d\zeta} + \dfrac{be_1}{2}T(-1) = R_i \\ -M_1(\zeta=-1) = B_1\dfrac{1}{L}\dfrac{du_1(-1)}{d\zeta} - D_1\dfrac{1}{L}\dfrac{d\theta_1(-1)}{dx} = S_i \end{cases} \quad \textbf{A-1}$$

Then, the expression of $-V_1(-1)$ is developed:

$$\begin{cases} -N_1(\zeta=-1) = -A_1\dfrac{1}{L}\dfrac{du_1(-1)}{d\zeta} + B_1\dfrac{1}{L}\dfrac{d\theta_1(-1)}{d\zeta} = Q_i \\ -V_1(\zeta=-1) = -B_1\dfrac{1}{L^2}\dfrac{d^2u_1(-1)}{d\zeta^2} + D_1\dfrac{1}{L^2}\dfrac{d^2\theta_1(-1)}{d\zeta^2} + \dfrac{be_1}{2}\dfrac{G_a}{e_a}\left(u_2(-1) - u_1(-1) - \dfrac{e_2}{2}\theta_2(-1) - \dfrac{e_2}{2}\theta_1(-1)\right) = R_i \\ -M_1(\zeta=-1) = B_1\dfrac{1}{L}\dfrac{du_1(-1)}{d\zeta} - D_1\dfrac{1}{L}\dfrac{d\theta_1(-1)}{d\zeta} = S_i \end{cases} \quad \textbf{A-2}$$

θ_1 and θ_2 are replaced by the third constitutive equation coming from (27).

$$\begin{cases} -N_1(\zeta=-1) = -A_1\dfrac{1}{L}\dfrac{du_1(-1)}{d\zeta} + B_1\dfrac{1}{L^2}\dfrac{d^2v_1(-1)}{d\zeta^2} = Q_i \\ -V_1(\zeta=-1) = -B_1\dfrac{1}{L^2}\dfrac{d^2u_1(-1)}{d\zeta^2} + D_1\dfrac{1}{L^3}\dfrac{d^3v_1(-1)}{d\zeta^3} + \dfrac{be_1}{2}\dfrac{G_a}{e_a}\left(u_2(-1) - u_1(-1) - \dfrac{e_2}{2}\dfrac{1}{L}\dfrac{dv_2}{d\zeta}(-1) - \dfrac{e_2}{2}\dfrac{1}{L}\dfrac{dv_1}{d\zeta}(-1)\right) = R_i \\ -M_1(\zeta=-1) = B_1\dfrac{1}{L}\dfrac{du_1(-1)}{d\zeta} - D_1\dfrac{1}{L^2}\dfrac{d^2v_1(-1)}{d\zeta^2} = S_i \end{cases} \quad \textbf{A-3}$$

The u_1, u_2, v_1 and v_2 are replaced by their expression in TEPS:

$$\begin{cases} -N_1(\zeta=-1) = \dfrac{A_1}{L}\displaystyle\sum_{n=0}^{+\infty}\frac{(n+1)!}{n!}(u_1)_{n+1}(-1)^n + \frac{B_1}{L^2}\sum_{n=0}^{+\infty}\frac{(n+2)!}{n!}(v_1)_{n+2}(-1)^n = Q_i \\ -V_1(\zeta=-1) = -\dfrac{B_1}{L^2}\displaystyle\sum_{n=0}^{+\infty}\frac{(n+2)!}{n!}(u_1)_{n+2}(-1)^n + \frac{D_1}{L^3}\sum_{n=0}^{+\infty}\frac{(n+3)!}{n!}(v_1)_{n+3}(-1)^n + \frac{be_1}{2}\frac{G_a}{e_a}\left(\sum_{n=0}^{+\infty}\left((u_2)_n - (u_1)_n - \frac{e_2}{2L}\frac{(n+1)!}{n!}(v_2)_{n+1} - \frac{e_1}{2L}\frac{(n+1)!}{n!}(v_1)_{n+1}\right)(-1)^n\right) = R_i \\ -M_1(\varphi=-1) = \dfrac{B_1}{L^2}\displaystyle\sum_{n=0}^{+\infty}\frac{(n+1)!}{n!}(u_1)_{n+1}(-1)^n - \frac{D_1}{L^2}\sum_{n=0}^{+\infty}\frac{(n+2)!}{n!}(v_1)_{n+2}(-1)^n = S_i \end{cases} \quad \textbf{A-4}$$

$$\begin{cases} -N_1(\zeta=-1)=\sum_{n=0}^{+\infty}\left[-\frac{A_1}{L}\frac{(n+1)!}{n!}(u_1)_{n+1}+\frac{B_1(n+2)!}{L^2\,n!}(v_1)_{n+2}\right](-1)^n=Q_i \\ -V_1(\zeta=-1)=\sum_{n=0}^{+\infty}\left[\left(-\frac{B_1}{L^2}\frac{(n+2)!}{n!}(u_1)_{n+2}+\frac{D_1}{L^3}\frac{(n+3)!}{n!}(v_1)_{n+3}\right)+\frac{be_1}{2}\frac{G_a}{e_a}\left((u_2)_n-(u_1)_n-\frac{e_2}{2L}\frac{(n+1)!}{n!}(v_2)_{n+1}-\frac{e_1}{2L}\frac{(n+1)!}{n!}(v_1)_{n+1}\right)\right](-1)^n=R_i \\ -M_1(\zeta=-1)=\sum_{n=0}^{+\infty}\left[\frac{B_1}{L^2}\frac{(n+1)!}{n!}(u_1)_{n+1}-\frac{D_1}{L^2}\frac{(n+2)!}{n!}(v_1)_{n+2}\right](-1)^n=S_i \end{cases} \quad \textbf{A-5}$$

The boundary conditions on the three other nodes are derived the same way.

Boundary condition on node j:

$$\begin{cases} -N_2(\zeta=-1)=\sum_{n=0}^{+\infty}\left[-\frac{A_2}{L}\frac{(n+1)!}{n!}(u_2)_{n+1}+\frac{B_2(n+2)!}{L^2\,n!}(v_2)_{n+2}\right](-1)^n=Q_j \\ -V_2(\zeta=-1)=\sum_{n=0}^{+\infty}\left[\left(-\frac{B_2}{L}\frac{(n+2)!}{n!}(u_2)_{n+2}+\frac{D_2}{L^3}\frac{(n+3)!}{n!}(v_2)_{n+3}\right)+\frac{be_2}{2}\frac{G_a}{e_a}\left((u_2)_n-(u_1)_n-\frac{e_2}{2L}\frac{(n+1)!}{n!}(v_2)_{n+1}-\frac{e_1}{2L}\frac{(n+1)!}{n!}(v_1)_{n+1}\right)\right](-1)^n=R_j \\ -M_2(\zeta=-1)=\sum_{n=0}^{+\infty}\left[\frac{B_2}{L^2}\frac{(n+1)!}{n!}(u_2)_{n+1}-\frac{D_2}{L^2}\frac{(n+2)!}{n!}(v_2)_{n+2}\right](-1)^n=S_j \end{cases} \quad \textbf{A-6}$$

Boundary condition on node k:

$$\begin{cases} N_1(\zeta=1)=\sum_{n=0}^{+\infty}\left[\frac{A_1}{L}\frac{(n+1)!}{n!}(u_1)_{n+1}-\frac{B_1(n+2)!}{L^2\,n!}(v_1)_{n+2}\right]=Q_k \\ V_1(\zeta=1)=\sum_{n=0}^{+\infty}\left[\left(\frac{B_1}{L}\sum_{n=0}^{+\infty}\frac{(n+2)!}{n!}(u_1)_{n+2}-\frac{D_1}{L^3}\frac{(n+3)!}{n!}(v_1)_{n+3}\right)-\frac{be_1}{2}\frac{G_a}{e_a}\left((u_2)_n-(u_1)_n-\frac{e_2}{2L}\frac{(n+1)!}{n!}(v_2)_{n+1}-\frac{e_1}{2L}\frac{(n+1)!}{n!}(v_1)_{n+1}\right)\right]=R_k \\ M_1(\zeta=1)=\sum_{n=0}^{+\infty}\left[-\frac{B_1}{L^2}\frac{(n+1)!}{n!}(u_1)_{n+1}+\frac{D_1(n+2)!}{L^2\,n!}(v_1)_{n+2}\right]=S_k \end{cases} \quad \textbf{A-7}$$

Boundary condition on node l:

$$\begin{cases} N_2(\zeta=1)=\sum_{n=0}^{+\infty}\left[\frac{A_2}{L}\frac{(n+1)!}{n!}(u_2)_{n+1}-\frac{B_2(n+2)!}{L^2\,n!}(v_2)_{n+2}\right]=Q_l \\ V_2(\zeta=1)=\sum_{n=0}^{+\infty}\left[\left(\frac{B_2}{L}\sum_{n=0}^{+\infty}\frac{(n+2)!}{n!}(u_2)_{n+2}-\frac{D_2}{L^3}\frac{(n+3)!}{n!}(v_1)_{n+3}\right)-\frac{be_2}{2}\frac{G_a}{e_a}\left((u_2)_n-(u_1)_n-\frac{e_2}{2L}\frac{(n+1)!}{n!}(v_2)_{n+1}-\frac{e_1}{2L}\frac{(n+1)!}{n!}(v_1)_{n+1}\right)\right]=R_l \\ M_2(\zeta=1)=\sum_{n=0}^{+\infty}\left[-\frac{B_2}{L^2}\frac{(n+1)!}{n!}(u_2)_{n+1}+\frac{D_2(n+2)!}{L^2\,n!}(v_2)_{n+2}\right]=S_l \end{cases} \quad \textbf{A-8}$$

References

[1] Hart-Smith, LJ. Design methodology for bonded-bolted composite joints. Technical Report, AFWAL-TR-81-3154, Douglas Aircraft Company, Long Beach, California, 1982.

[2] Kelly, G. Quasi-static strength and fatigue life of hybrid (bonded/bolted) composite single-lap joints. Compos. Struct., 2006, 72, 119-129.

[3] da Silva, LFM, Öschner, A, Adams, RD (Editors). Handbook of Adhesion Technology (2 volumes), 2nd edition Springer, Heidelberg, Germany, 2018.

[4] Carbas, RJC, da Silva, LFM, Critchlow, GW. Adhesively bonded functionally graded joints by induction heating. Int. J. Adhes. Adhes., 2014, 48, 110–118.

[5] Carbas, RJC, da Silva, LFM, Madureira, ML, Critchlow, GW. Modelling of functionally graded adhesive joints. J. Adhesion, 2014, 90(8), 698-716.

[6] Carbas, RJC, da Silva, LFM, Andrés, LFS. Functionally graded adhesive joints by graded mixing of nanoparticles. Int. J. Adhes. Adhes., 2017, 76, 30–37.

[7] Paroissien, E., da Silva, L.F.M., Lachaud, F.. Simplified stress analysis of functionally graded single-lap joints subjected to combined thermal and mechanical loads. Compos. Struct., 2018, 203, 85-100.

[8] Marques, JB, Barbosa, AQ, da Silva, CI, Carbas, RJC, da Silva, LFM. An overview of manufacturing functionally graded adhesives – Challenges and prospects. The Journal of Adhesion, 2019, DOI: 10.1080/00218464.2019.1646647

[9] Kawasaki, S, Nakajima, G, Haraga, K, Sato, C. Functionally Graded Adhesive Joints Bonded by Honeymoon Adhesion Using Two Types of Second Generation Acrylic Adhesives of Two Components. J. Adhesion, 2016, 92(7-9), 517-534.

[10] Durodola, JF. Functionally graded adhesive joints – A review and prospects. Int. J. Adhes. Adhes., 2017, 76, 83-89.

[11] Breto, R, Chiminelli, A, Duvivier, E, Lizaranzu, M, Jiménez, MA. Finite Element Analysis of Functionally Graded Bond-Lines for Metal/Composite Joints. J. Adhesion, 2015, 91, 920-936.

[12] Stein, N, Weißgraeber, P, Becker, W. Stress solution for functionally graded adhesive joints. Int. J. Solids Struct., 2016, 97-98, 300-311.

[13] Stein, N, Felger, J, Becker, W. Analytical models for functionally graded adhesive joints: A comparative study, Int. J. Adhes. Adhes., 2017, 76, 70-82.

[14] Paroissien, E. Contribution aux Assemblages Hybrides (Boulonnés/Collés) – Application aux Jonctions Aéronautiques. PhD Thesis (in French), Université de Toulouse III, 2006.

[15] Paroissien, E, Lachaud, F, da Silva, LFM, Seddiki, S. A comparison between macro-element and finite element solutions for the stress analysis of functionally graded single-lap joints. Compos. Struct, 2019**,** 215, 331-350.

[16] Hart-Smith, LJ.. Adhesive-bonded scarf and stepped-lap joints, 1973.

[17] Volkersen, O. Die Nietkraftverteilung in Zugbeanspruchten Nietverbindungen mit konstanten Laschenquerschnitten, Luftfahrforschung, 1938. 15(24), 41-47.

[18] Goland, M, Reissner, E. The stresses in cemented joints, J. Appl. Mech., 1944, 11, A17-A27.

[19] Hart Smith, RJ. Adhesive-bonded double-lap joint. NASA Technical Report, 1973. CR-112235.

[20] Weissgraeber, P, Stein, N, Becker, W. A general sandwich-type model for adhesive joints with composite adherends. Int. J. Adhes. Adhes, 2014. 55, 56–63.

[21] Clarke, JLM. Structural Design of Polymer Composites: Eurocomp Design Code and Background Document, second ed, 2003. CRC Press, ISBN 203475135.

[22] Lelias, G, Paroissien,E, Lachaud, F, Morlier, J, Schwartz, S, Gavoille, C. An extended semi-analytical formulation for fast and reliable mode I/II stress analysis of adhesively bonded joints. Int. J. Solids Struct, 2015. 62 18–38